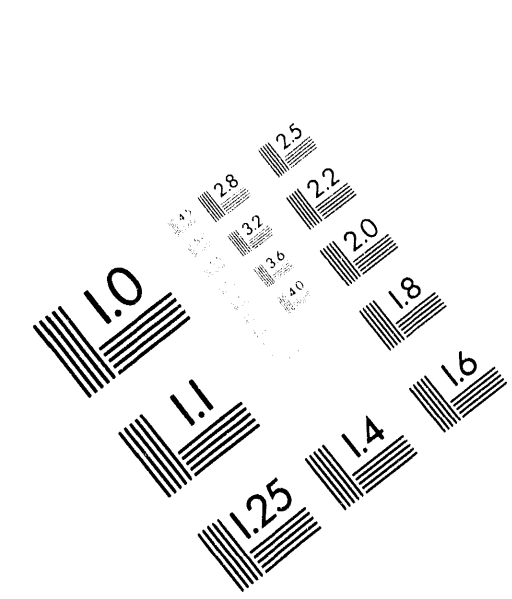

Association for Information and Image Management

1100 Wayne Avenue, Suite 1100
Silver Spring, Maryland 20910
301/587-8202

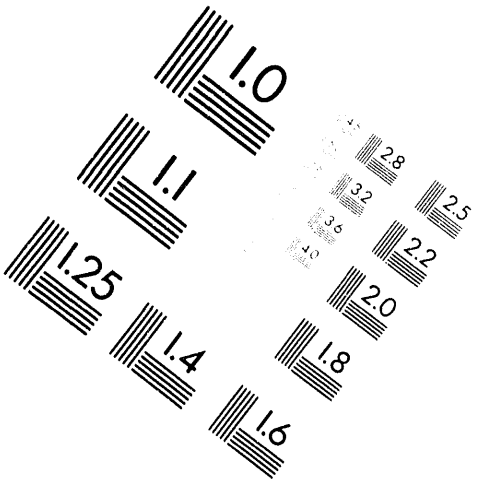

Centimeter

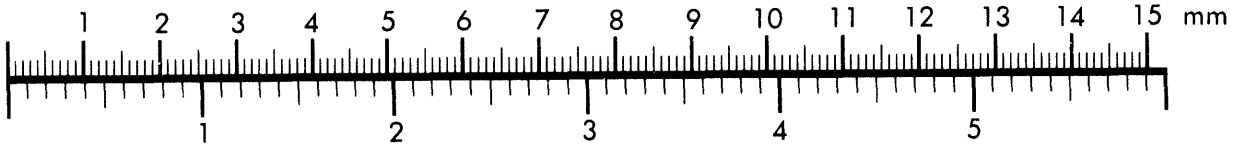

Inches

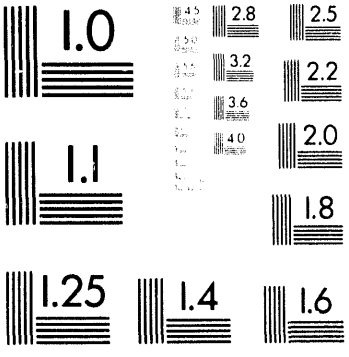

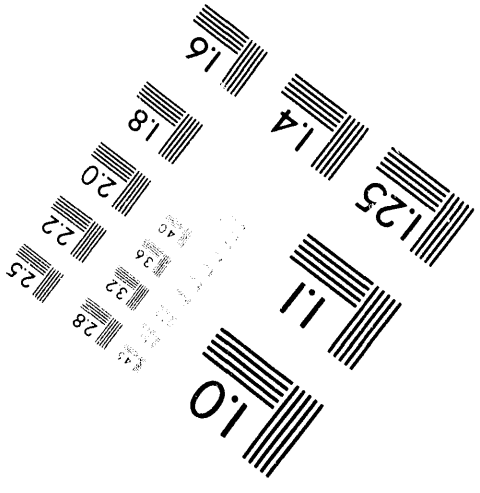

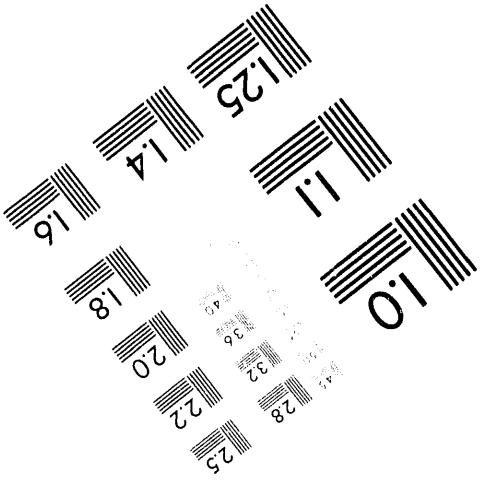

MANUFACTURED TO AIIM STANDARDS
BY APPLIED IMAGE, INC.

1 of 1

SAND--94-8501C
Conf-940838--4

INFLUENCES OF FLAME–VORTEX INTERACTIONS ON FORMATION OF OXIDES OF NITROGEN IN CURVED METHANE–AIR DIFFUSION FLAMELETS

JOHN M. CARD

Combustion Research Facility, MS 9051

Sandia National Laboratories, Livermore, California 94551-0969 USA

ROLAND RYDÉN

Combustion and Aerodynamics

Volvo Flygmotor, S-46181 Trollhättan, Sweden

and

FORMAN A. WILLIAMS

Center for Energy and Combustion Research

University of California, San Diego, La Jolla, California 92093-0310 USA

Correspondence: All correspondence should be directed to J. M. Card at the above address, Tel: (510) 294-1354, Fax: (510) 294-1004, E-mail: jmcard@ca.sandia.gov

Word Count:	5 Figures + 1 Table:	1200 words
	Text and Eqs.:	4047 (9 1/2 pages @ 426 words/page)
	Refs.:	267
	Total:	5514 words

Presentation Preference: Oral

Publication Preference: Proceedings

General Approach: A. Theory

Subjects: (1.3) Combustion Chemistry – Reduced Reaction Mechanisms
(3.9) Flames – Flame/Vortex Interactions
(10.4) Environmental Studies – NO_x

INFLUENCES OF FLAME–VORTEX INTERACTIONS ON FORMATION OF OXIDES OF NITROGEN IN CURVED METHANE–AIR DIFFUSION FLAMELETS

JOHN M. CARD

Combustion Research Facility

Sandia National Laboratories, Livermore, California 94551-0969 USA

ROLAND RYDÉN

Combustion and Aerodynamics

Volvo Flygmotor, S-46181 Trollhättan, Sweden

and

FORMAN A. WILLIAMS

Center for Energy and Combustion Research

University of California, San Diego, La Jolla, California 92093-0310 USA

Abstract

To improve knowledge of rates of production of oxides of nitrogen in turbulent diffusion flames in reaction-sheet regimes, an analytical investigation is made of the structure of a flamelet having a parabolic shape. The mixture-fraction field, the scalar dissipation rate and the gas velocity relative to the flamelet in the vortex are related to the flame curvature at the tip of the parabola. The flame structure for major species and for temperature is described by rate-ratio asymptotics based on two-step and three-step reduced chemical-kinetic mechanisms. Production rates by prompt, thermal and nitrous-oxide mechanisms are obtained from one-step reduced-chemistry approximations that employ steady states for all reaction intermediaries. For sufficiently large streamwise separation distances between isoscalar surfaces it is found that equilibrium conditions are closely approached near the flame tip, and the thermal mechanism dominates there, but the prompt mechanism always dominates in the wings, away from the tip, where the highest rates of scalar dissipation occur. Increasing the tip curvature increases the Péclet number and the prompt contribution while decreasing the thermal contribution. At 1 atm and ambient temperatures of 300 K, the prompt mechanism always dominates the total production rate in the parabolic flamelet, and, perhaps surprisingly, the rate of the nitrous-oxide mechanism is faster than that of the thermal mechanism and varies with the tip curvature and with scalar dissipation in the same manner as that of the prompt mechanism, different from that of the thermal mechanism. The general conclusion reached is that Zel'dovich NO is relatively insignificant in hydrocarbon–air mixtures in reaction-sheet regimes.

Introduction

Interest in reducing pollutant emissions from gas burners motivates studies of rates of production of oxides of nitrogen in turbulent hydrocarbon–air diffusion flames. Although detailed kinetics and rate constants have been published and applied to laminar flames and stirred reactors [1–3], uncertainties in turbulence modeling cast great doubt on applications of these results to turbulent combustion. Since direct numerical simulation with detailed chemistry at turbulence Reynolds numbers of interest will remain beyond computational speed and memory capacities for many years, there is a need for obtaining reliable simplified descriptions of NO_x production rates in turbulent flows that may improve understanding and also possibly lead to useful computational methods. The reaction-sheet regime [4] of turbulent combustion is one in which simplification can be achieved by first addressing production rates in laminar flamelets then summing those rates over suitable statistical ensembles, as was attempted in one recent study [5]. The present paper addresses such flamelet production rates for turbulent methane–air diffusion flames.

Previous studies along these lines [5] selected planar counterflow diffusion flamelets as the laminar subelements in which the NO_x production occurred. Questions arise as to whether this selection overlooks potentially important influences of flamelet curvature. For jet diffusion flames, it has been shown [6, 7] that except at impractically large Péclet numbers $\mathrm{Pe} = \Gamma/D$ (where Γ is the circulation of a vortex and D a characteristic diffusion coefficient) diffusion flames wrap only part way around vortices then experience a period of quasisteadiness, rather than penetrating to form a reacted core [8, 9]. A parabolic flame in uniform flow (Fig. 1) has recently been identified as an excellent analytical approximation to the quasisteady, partially wrapped diffusion flame [10]. The fidelity of this approximation for describing flamelet structures in the vicinity of the flame tip has been tested by rate-ratio asymptotics and by numerical simulation [10] and has been found to be excellent. The present study exploits this parabolic-flame approximation to simplify the investigation of influences of flamelet curvature on NO_x production. Attention is restricted to individual flamelets of parabolic shape, and questions of how to incorporate the results into descriptions of turbulent diffusion flames are not addressed.

Fig. 1

Previous NO_x and curved-flame studies [5, 10] employing rate-ratio asymptotics for hydrocarbon–air diffusion flamelets relied on a two-step chemistry approximation involving separate fuel-consumption and oxygen-consumption steps. However, it is known (cf. [11]) that at least a three-step mechanism that allows, additionally, for water-gas nonequilibrium is required for obtaining good accuracy in predictions of extinction of methane–air diffusion flames. For this reason, since the parabolic flamelets are stretched towards extinction in their wings, the three-step chemistry is employed in the present work. The results of the three-step and two-step descriptions are compared, to ascertain consequent influences on NO_x production rates. In addition, results of new computations

are reported for planar, counterflow flames with a detailed chemical-kinetic mechanisms, to enable comparisons with the reduced-chemistry predictions to be made.

The Parabolic Flamelet

Postulating a thin reaction zone, we assume Lewis numbers of unity for all species in the external transport zones, so that a simple mixture fraction Z can be introduced, having the values 0 and 1 in oxidizer and fuel streams, respectively, and obeying a source-free, time-dependent, convective-diffusive balance [12]. As seen from the outer Z variable, the combustion chemistry occurs at the stoichiometric surface $Z = Z_{st}$, where $Z_{st} = (1 + 2W_{O_2}/(W_{CH_4}Y_{O_2\infty}))^{-1}$ is the stoichiometric mixture fraction for the oxidation of methane, in which W_i is the molecular weight of species i, $Y_{O_2\infty}$ is the oxygen mass fraction in the oxidizer stream, and the fuel mass fraction is unity at $Z = 1$.

Even with an assumption of infinite-rate chemistry, the spatially multidimensional and time-dependent nature of diffusion flamelets in swirling flows must, in general, be described numerically [6]. However, it has been shown [7] that when a period of quasisteadiness occurs, a flame tongue is formed, and its shape can be idealized as a stretched parabola [10]. We therefore approximate the shape of the flamelet (Fig. 1), for $0 \le Z \le 1$, as $Z = \kappa x^2/(2l) - y/l$, in which κ is a parameter that measures the curvature at the tip of the flamelet, and l is the vertical distance between the $Z = 0$ (oxidizer-stream) and $Z = 1$ (fuel-stream) boundaries. In addition, if the product ρD is assumed to be a constant, where ρ is the gas density and D is the common diffusion coefficient for all species and enthalpy, then the magnitude of the swirl velocity V of the imposed velocity field (see Fig. 1) is related to κ by the expression $V = \kappa D$, derived from the conservation equation for Z [10]. The swirl velocity can also be related to the circulation Γ for a point vortex by the expression $\Gamma = 2\pi r V$, where r is the vortex radius. From these results, it can readily be deduced that the previously defined Péclet number can be expressed as $Pe = 2\pi r\kappa$.

It is convenient to introduce the rate of scalar dissipation, $\chi = 2D\,|\nabla Z|^2$, to characterize the flow-field effects on the flamelet. With the adopted assumptions, it has been shown [10] that for the parabolic flamelet χ is given by

$$\chi = (2D/l^2)[1 + (\kappa x)^2], \tag{1}$$

and for surfaces of constant Z the arc length S from the tip of the flamelet is

$$S(x) = \left\{\kappa x\sqrt{1 + (\kappa x)^2} + \ln\left(\kappa x + \sqrt{1 + (\kappa x)^2}\right)\right\}/(2\kappa), \tag{2}$$

where we need only consider $x \ge 0$, because of the symmetry of the presumed Z field. The analysis for the structure of the reaction zone proceeds most easily by transforming from physical space

to an orthogonal coordinate system in mixture-fraction space, so that Z becomes an independent variable normal to the flame surface, and the other two coordinates are perpendicular to ∇Z. The species-conservation equation is then transformed to

$$\rho\frac{\partial Y_i}{\partial t} + \rho \mathbf{v}_\perp \cdot \nabla_\perp Y_i - \nabla_\perp \cdot (\rho D \nabla_\perp Y_i) = \mathrm{w}_i + \frac{\rho\chi}{2}\frac{\partial^2 Y_i}{\partial Z^2}, \tag{3}$$

where $\mathbf{v}$ is the gas velocity, Y_i the mass fraction of species i, w_i the net mass rate of production of species i, and the subscript $\perp$ refers to the S coordinate along surfaces of constant Z. A similar expression applies to energy conservation.

The terms on the left-hand side of Eq. 3 represent temporal variations and convection and diffusion along the reaction sheet, respectively. Here we neglect time variations, because of the assumed quasisteadiness, and, for typical swirling-flow conditions, order-of-magnitude estimates indicate that the transverse diffusive term is small relative to the other terms and that the effects of transverse convection are important only near (but not at) the flame tip and only when κ is large [10], so that this may be neglected in the present study, since we only consider mild curvature. Consequently, only the terms on the right-hand side of Eq. 3, representing the typically assumed reactive-diffusive balance, are included. However, an order-of-magnitude estimate at the end of the discussion assesses whether a convective-diffusive-reactive balance may develop and alter the NO_x history.

Reduced Chemistry for Flame Structure

The method of rate-ratio asymptotics (cf. [4]) is employed to analyze the structures of methane-air diffusion flamelets, here with a three-step reduced mechanism for the fuel chemistry, in which the only rate constants needed are those appearing in Table 1 [13], where the numbering of steps is selected to agree with Ref. [13], which may be consulted along with Ref. [14] for further details of the flame-structure analysis. These rate constants are more recent and differ slightly from those used in our earlier work. Since the nitrogen chemistry has negligible influence on the main flame structure, the analysis of structure and extinction can be completed prior to consideration of NO_x production. Table 1

The flamelet structure in mixture-fraction space is illustrated in Fig. 2 for the two-step approximation, where there is a reaction zone consisting of two layers. On the fuel-rich side is a fuel-consumption layer, scaled by the small parameter δ, where CH_4 is attacked by radicals to form H_2 and CO. The stoichiometry of the fuel-consumption step is $CH_4 + O_2 \rightarrow CO + H_2 + H_2O$ (I), with a corresponding rate $\omega_\mathrm{I} = k_{38f}[CH_4][H]$. On the lean side is an oxidation layer, scaled by the small parameter $\epsilon > \delta$, in which H_2 and CO are oxidized to form CO_2 and H_2O along with the production of radicals. The global step here is $O_2 + 2H_2 \rightarrow 2H_2O$ (III), and its rate is $\omega_\mathrm{III} =$ Fig. 2

$k_{5f}[\mathrm{H}][\mathrm{O}_2][M]$. In the three-step approximation, there is an additional layer, scaled by the small parameter ν ($\delta < \nu < \epsilon$), that is embedded between the fuel-consumption and oxygen-consumption layer. It is only in this layer that the nonequilibrium effects of the water-gas shift reaction $\mathrm{CO} + \mathrm{H}_2\mathrm{O} \rightleftharpoons \mathrm{CO}_2 + \mathrm{H}_2$ (II) are assumed to occur; the rate is $\omega_{\mathrm{II}} = (k_{18f}/K_3)[\mathrm{H}]([\mathrm{CO}][\mathrm{H}_2\mathrm{O}]/[\mathrm{H}_2] - [\mathrm{CO}_2]/(K_{18}/K_3))$. In the above expressions, the K's are equilibrium constants, the concentration of H is $[\mathrm{H}] = (1 - k_{38f}[\mathrm{CH}_4]/(k_{1f}[\mathrm{O}_2]))^{1/2}[\mathrm{O}_2]^{1/2}[\mathrm{H}_2]^{3/2}(K_1K_2)^{1/2}K_3/[\mathrm{H}_2\mathrm{O}]$, which is obtained by introducing the steady-state approximation for H, and the concentration of the third body is $[M] = p\overline{W}/(RT)\sum_i(\eta_i Y_i/W_i)$, where $i = \mathrm{N}_2, \mathrm{CO}_2, \mathrm{H}_2\mathrm{O}$, in which $\eta_i = 0.4, 1.5, 6.5$ are their respective catalytic efficiencies [13], and where p is pressure, R is the universal gas constant, and the average molecular weight $\overline{W}$ is approximated as that of nitrogen, W_{N_2}.

Simplified Mechanism for NO Formation

Two recent studies of reduced chemistry for NO_x formation are those of Glarborg et al. [3] who treated methane combustion in perfectly stirred reactor and of Røkke et al. [5] who considered hydrocarbon–air diffusion flames. Since our problem concerns diffusion flames, the latter approach clearly is more appropriate for our purposes. In following the earlier [5] methodology, it becomes necessary here only to summarize results. However, various misprints and errors in the previous publication [5] are corrected here.

The last three entries in Table 1 are the elementary rate constants for the initiation steps for the thermal (Zel'dovich,Z), nitrous-oxide (N) and prompt (P) mechanisms. The rates (mol/cm^{3}s) for the overall process $\mathrm{N}_2 + \mathrm{O}_2 \rightarrow 2\mathrm{NO}$, as controlled mainly by each of these steps, are denoted by ω_{Z}, ω_{N} and ω_{P}, respectively. Especially for the $\mathrm{N}_2\mathrm{O}$ route, the initial step may not be followed by complete conversion to NO; ω_{N} actually represents the formation rate of $\mathrm{N}_2\mathrm{O}$ (an undesirable species, like NO), and the ultimate fate of this molecule is not considered. For the prompt route, ω_{P} depends on rate constants for other steps as well [5], and the previously published [5] values for these steps will be employed here. The entries in Table 1 for Z and P are the same as earlier [5], obtained from Miller and Bowman [1], but those for N differ. An error in the previous study [5] assigned 25 rather than 15 kcal/mol as the activation energy for step N, derived from data in Ref. [1], correcting this error significantly increases the estimated [5] contribution from the $\mathrm{N}_2\mathrm{O}$ route, but the qualitative conclusions (e.g. that the other two routes dominate for the situations considered) are unchanged. In Table 1 for step N, following Ref. [2], the rate parameters of Hanson and Salimian [15] are selected, as supported by more recent work [16], rather than results from Ref. [1], used elsewhere [3], which give rates too high.

For both the thermal and nitrous-oxide mechanisms, a steady state for O and partial equilibria for $\mathrm{H} + \mathrm{O}_2 \rightleftharpoons \mathrm{OH} + \mathrm{O}$ and $\mathrm{OH} + \mathrm{H}_2 \rightleftharpoons \mathrm{H}_2\mathrm{O} + \mathrm{H}$ are introduced, with the further approximation that

$[H_2] = [H_2O]/5$, so that only major-species concentrations appear in the resulting rate expressions, giving $\omega_2 = 9 \times 10^{12} T^{0.3} e^{-38,440/T}[N_2][O_2]$ and $\omega_N = 6.78 \times 10^{12} e^{-10,423/T}[N_2][O_2][\tilde{M}]$. For the prompt, steady-state approximations are introduced for the species H, CH, CH_2 and C_2H_2, along with the partial-equilibrium assumption for $CH_4 + H = CH_3 + H_2$, thereby yielding

$$\omega_P = \left\{ \frac{3 \times 10^{10} e^{-2900/T} F^{3/2} G[N_2][CH_4][O_2]^{3/2}[H_2O]^{1/2}}{([\tilde{M}] - [N_2])([\tilde{M}] - [N_2] - [\tilde{C}])} \right\} (1 + 3000\epsilon^{-15,185/T}),$$

where $F = 1 - 1.1 \times 10^{-10} T^3 e^{4051/T}[CH_4]/[O_2]$, and $G = 1 + 40e^{-5900/T} + 2.6 \times 10^{13} pT^{-4} e^{7600/T} \times [CH_4]/[H_2O]$, and where $[\tilde{M}] \approx p/RT$, and $[\tilde{C}]$ is the concentration of species containing C atoms; for the present analysis, we assume $[\tilde{C}] \approx [CO_2]$. On the last line of Eq. 3 of Ref. [5], negative signs belong before 2450 and 15,185, and in Eq. 4, $[CH_4]/[H_2O]$ should be $[C_3H_8]/[O_2]$. The rate constants that implicitly appear above are slightly different than those used for the fuel kinetics, as listed in Table 1, but resulting differences in calculating ω with either set of constants are less than 10%, well within the factor of two of uncertainty for the Zel'dovich and nitrous-oxide mechanisms and the factor of ten of uncertainty for the prompt path.

Summary of Asymptotic Analysis

The inputs required for calculating ω are provided here by rate-ratio asymptotics with the three-step reduced approximation having the ordering $\delta < \nu < \epsilon < 1$. Since details of the method may be found in earlier investigations [11,17-20], we present only the results of the analysis and exhibit the formulas needed to obtain the necessary inputs.

Appropriate expansions are introduced such that the scaled concentration of H_2, defined as z^0, may be found at the scaled flame location ξ_0; a solution for $z^0 \equiv z^0(\xi_0)$, empirically fitted to the results of the oxidation-layer analysis, is $z^0 = \xi_0 + 0.9\sqrt{\xi_0^2 - 1.3\xi_0 + 1.5}$. The flame temperature $T = T^0$ is found to be $T^0 = T_{st} + \Theta\epsilon(a\xi_0 - 2bqz^0)$, where $a \equiv W_{N_2}/W_{CH_4}$ and $b \equiv Y_{O_2\infty} W_{N_2}/(2W_{O_2} Z_{st})$ are obtained from matching to the solution of the outer structure, $q \approx 0.33$ is a normalized energetic parameter for the average heat release for the oxidation of CO and H_2, and $\Theta \approx 20,000$ K is a parameter related to the total heat release per mole of methane. The scaling parameter ϵ for the oxidation layer is

$$\epsilon \equiv \left\{ \lambda^0 X^0_{H_2O} W_{N_2} (1 + \alpha^0)^{3/2} / [16 b^2 \rho^0 k_{5f} [M]^0 (K_1^0 K_2^0)^{1/2} K_3^0 (L_{O_2} L_{H_2})^{3/2}] \right\}^{1/4} \qquad (4)$$

where L_i is the Lewis number of species i, and $\alpha = X_{CO_2} L_{H_2} K_3/(X_{H_2O} L_{CO} K_{18})$, in which $X_i = Y_i W_{N_2}/W_i = [i](RT/p)$, since $\overline{W} \approx W_{N_2}$. The coupling relations for CO_2 and H_2O give $[CO_2]^0 = (\rho^0/W_{N_2})[0.095 + L_{CO_2}\epsilon(a\xi_0 - 2b\alpha^0 z^0/(1 + \alpha^0))]$ and $[H_2O]^0 = (\rho^0/W_{N_2})[0.19 + 2L_{H_2O}\epsilon(a\xi_0 - bz^0/(1 + \alpha^0))]$, respectively, while, approximately, $[N_2]^0 = 0.0255\rho^0$, and from O-coupling, $[O_2]^0 = (2L_{O_2} b\epsilon\rho^0/W_{N_2})(z^0/2 - \xi_0)$.

The asymptotic analysis of the oxygen-consumption zone provides an explicit relation for the rate of scalar dissipation, namely

$$\chi^0 = \frac{16\rho^0 k_{5f}^0 [M]^0 b^2 (K_1^0 K_2^0)^{1/2} K_3^0 (L_{O_2} L_{H_2})^{3/2} (T_{st} - T^0)^4}{X_{H_2O}^0 (1+\alpha^0)^{3/2} W_{N_2} \Theta^4 (2bqz^0 - a\xi_0)^4}. \tag{5}$$

In addition, by including results of the analysis of the fuel-consumption zone, the expression

$$\frac{(k_{1f}^0)^2 L_{O_2}}{k_{38f}^0 k_{5f}^0 [M] L_{CH_4}} (z^0)^4 \left(1 - \frac{2\xi_0}{z^0}\right)^{5/2} \left(1 - \frac{\nu(1+\alpha^0)}{2\epsilon z^0}\right) = \frac{15}{(2)^{3/2}} \tag{6}$$

is obtained, where expansions for nonequilibrium of the water gas-shift have been introduced, in which

$$\nu \equiv \left\{\chi^0 W_{N_2} (1-\alpha^0)^2 / [2(1+\alpha^0)^3 k_{18f} \rho^0 (K_1^0 K_2^0)^{1/2} (X_{O_2}^0 X_{H_2}^0)^{1/2} L_{CO}]\right\}^{1/2}. \tag{7}$$

The concentration of the fuel in the reaction zone is approximated by $[CH_4]^0 \approx (1/2)\delta b L_{CH_4} \rho^0 / W_{N_2}$, where

$$\delta \equiv k_{1f}^0 X_{O_2}^0 / (L_{CH_4} b k_{38f}^0). \tag{8}$$

Variation of the temperature and of the rate of scalar dissipation in the reaction zone have been neglected in the above results, since studies have indicated [11, 19] that, regardless of the flow-field configuration, these variations have a negligible influence on the solution.

The method of calculating flamelet NO_x production has been presented previously [5]. The quantity most directly relevant is the integrated rate across the mixture fraction, $\hat{\omega} = \int_0^1 \omega dZ$. For the prompt mechanism, ω_P is approximated as a constant, ω_P^0 throughout the fuel-consumption layer, giving $\hat{\omega}_P = \delta\omega_P^0$. For the other two mechanisms, activation-energy asymptotics may be employed, resulting in [5]

$$\hat{\omega} = \frac{\omega^0}{(n + T_A/T^0)} \left[\frac{1 - Z_0}{1 - T_o/T^0} + \frac{T^0}{a\Theta(1 - 2bq/a)}\right],$$

where T_A is the activation temperature (E/R^o), n the temperature dependence of the preexponential factor (Table 1), and T_o the inlet temperature of the oxidizer stream (equal to the fuel-stream inlet temperature T_f), here taken to be 300 K. Consideration of the next term in the asymptotic expansion suggests that this last formula is accurate for the Zel'dovich mechanism but overestimates nitrous-oxide production rates by about 10%.

Calculation Procedure

The calculations were performed first by selecting T^0 and then determining ξ_0, z^0, ϵ, $X_{O_2}^0$, δ, $X_{H_2O}^0$, $X_{CO_2}^0$, α^0, $X_{H_2}^0$, χ^0, ν, and Z_0; details of the computational procedure may be found in an earlier paper [10]. Results for two-step chemistry were readily obtained from the three-step results by

putting $\nu = 0$. In the reaction layer, the influences of nonunity Lewis numbers are taken into account, assigning CH_4, O_2, CO_2, H_2O, CO and H_2 the Lewis numbers 0.97, 1.11, 1.39, 0.83, 1.1, and 0.3, respectively [14]. In all calculations here, $p = 1$ atm. For methane in air ($Z_{st} = 0.055$), the peak flame temperature is $T_{st} = 2320$ K [11]. Values for κ and l were chosen to assure that the effects of transverse convection need not be considered (typically $\kappa \leq 20$ cm^{-1}) [10]. The x coordinate is then obtained from χ by use of Eq. 1, where $D \approx 4$ cm^2/s [19], and the distance S from the flame tip can then be found from Eq. 2. Since the flame-structure analysis provides χ^0, independent of the flow field, the effects of the flow configuration are introduced by evaluating χ in Eq. 1 at $Z = Z_{st}$, namely [10],

$$\chi_{st} = (\chi^0/(1+(\kappa x)^2))\left\{1+[\kappa x(1-\epsilon\xi_0 l\kappa/(1+(\kappa x)^2))]^2\right\}. \qquad (9)$$

Results

The variations of T^0 and χ_{st} with the arc distance S are shown in Fig. 3. The relevant flame-shape parameters, varied here, are l and κl. The general behavior of T^0 and χ_{st} with varying l and κl ($\sim Pe$) is identical to that found in our earlier study [10], where rough estimates of Pe are made by assuming that the vortex-tube radius is approximately 1 cm [21]. The flamelet temperature and scalar dissipation at the flame tip are independent of κ or Pe if l is not allowed to vary. Away from the tip, larger values of Pe result in a larger χ_{st} (and hence lower T^0) at a given S, thereby producing a more highly strained flame that extinguishes at smaller values of S; henceforth S_q denotes the distance at which the flame quenches. Similarly, decreasing l also results in a more highly strained flame, since smaller values of l effectively increases ∇Z, resulting in a larger χ_{st}. Fig. 3

Illustrated in Fig. 4 is the variation of $\hat{\omega}_P$ with S for various κ and l. Since the highest flame temperatures and the smallest concentration of fuel occur at the tip, the smallest values of $\hat{\omega}_P$ are found there. But as S approaches S_q, where lower flame temperatures and higher concentrations of fuel occur, $\hat{\omega}_P$ rapidly increases. As expected, varying κ has no influence at the tip when l is fixed. However, by increasing l the rate of scalar dissipation decreases (and the concentration of fuel decreases), resulting in smaller rates of production of NO though the prompt path. Far from the tip, the behavior of $\hat{\omega}_P$ is similar to that described for T^0, where for a fixed κ, extinction occurs at larger values of S as l is increased. When the spacing l is held constant, smaller κ results in more robust flames in the wings. The influences of T^0, $[O_2]^0$ and $[CH_4]^0$ are readily seen through the earlier expression for ω_P, where the larger values of $[O_2]^0$ and $[CH_4]^0$ near extinction causes ω_P to increase. If the elementary rate constant of Glarborg et al. [3] for step P were employed here, $\hat{\omega}_P$ would be about a factor of two larger than shown in Fig. 4 for S near zero and about 20% larger for $S \rightarrow S_q$; these differences are less than rate-constant uncertainties. Fig. 4

Figure 5 shows $\hat{\omega}_Z$ and $\hat{\omega}_N$ as functions of S. The observed decrease in ω_z with distance from the flame tip is expected since the activation energy is quite large, even though the increasing leakage of oxygen through the reaction zone as extinction is approached mitigates the effect of decreasing temperature. Perhaps surprisingly, on the contrary $\hat{\omega}_N$ increases monotonically as S increases, the leakage of oxygen being large enough to offset the moderately large activation energy. In both cases, varying κ and l shifts the curves in a manner readily inferred from that described above for the prompt path and for T^0 and χ_{st}. There is good agreement in the literature on the elementary rate parameters for step Z, but for step N, if the rate constants reported by Glarborg et al. [3] are used instead of those in Table 1, then $\hat{\omega}_N$ is increased by roughly a factor of three. Fig. 5

Discussion

How important was it to proceed from the two-step [10] to the present three-step flame-chemistry description? Not tremendously important for local NO_x. For example, at $T^0 = 1700$ K, $\hat{\omega}_P$ is about 30% lower and $\hat{\omega}_N$ and $\hat{\omega}_Z$ about 10% lower for the two-step approximation, and at $\chi_{st} = 20\ s^{-1}$, with two steps $\hat{\omega}_P$ is about 60% less, $\hat{\omega}_N$ about 13% less and $\hat{\omega}_Z$ about 40% higher (because of the higher temperature). These results are representative of maximum errors since near the tip, where T^0 is larger and χ_{st} smaller, the discrepancies are much less. Thus, at a given T^0 or χ_{st}, the ν terms have relatively little influence on $\hat{\omega}$, less of an effect than the uncertainties in the $\hat{\omega}$ formulas. This conclusion is favorable in suggesting that relatively simple reduced flame chemistry can be used in NO_x estimates, and previous results [5] do not suffer much of a penalty from their two-step flame-chemistry approximation. However, χ_{st} at extinction is nearly an order of magnitude too large in the two-step approximation, so S_q and correspondingly the total NO_x production rate per parabolic flamelet would be much too large; it is always necessary to extinguish the flamelet at the proper χ_{st}, as the three-step approximation does.

Our retention of only the reactive-diffusive balances eliminates the possibility of prompt NO, produced in the wings, being swept convectively towards the tip to swamp out the thermal NO produced there. Conditions under which this occurs may be estimated in terms of a diffusion time, $t_d = \epsilon^2/\chi_{st}$, and a convective time, $t_c = \Delta/V_t$, where $\Delta \approx 0.1$ cm (a typical distance at which the prompt path becomes dominant) and $V_t \approx V$ is the tangential velocity along the flamelet. If near the tip $\epsilon \approx 0.01$ and $\chi_{st} \approx 1\ s^{-1}$, so that $t_d \approx 1 \times 10^{-4}$ s, then t_d becomes within an order of magnitude of t_c when $V_t > 100$ cm/s. Thus, for swirl velocities V exceeding about 100 cm/s, corresponding to Péclet numbers greater than about 500, it may be sufficient to consider just the prompt path for estimating NO_x emissions. Our present considerations concern smaller values of V, which are estimated to be representative of the majority of the applications.

Since we maintain a reactive-diffusive balance, planar counterflow flamelets can be considered for

assessing the accuracy of our reduced-chemistry description of NO_x production. A few computations with full chemistry have been published for NO production in counterflow methane–air diffusion flames [22, 23], but the integral $\hat{\omega}$, which is calculated from the asymptotics, is not extractable from the numerical results reported. Therefore, additional counterflow numerical computations were made, using the seventy-some-step mechanism of Glarborg et al. [3], but with Z, N and P rate parameters of Table 1; details of the computation procedure appear in Ref. [24], for example. Comparisons of peak and integrated production rates (in units of 10^{-6} mol/cm^{3}s) are give below:

	χ_{st} = 0.5 s^{-1}			5			15		
	P	Z	N	P	Z	N	P	Z	N
Asymptotics ω_{max}	8.1	0.34	0.10	35	0.18	0.15	100	0.08	0.19
Numerics ω_{max}	0.62	0.25	0.11	1.6	0.12	0.09	0.01	0.0002	0.0007
Asymptotics $\hat{\omega} \times 10^3$	8.7	24	23	81	11	36	350	5.0	43
Numerics $\hat{\omega} \times 10^3$	2.2	2.3	0.65	3.8	1.2	0.64	0.3	0.002	0.01

These comparisons show agreement only in general trends, at best; the asymptotic results would appear to overestimate production rates appreciably, especially for the prompt mechanism at high χ_{st}, where the differences, approaching three orders of magnitude, exceed even the large uncertainties in the elementary rates. The asymptotic trends of increasing $\hat{\omega}_P$ and $\hat{\omega}_N$ with increasing χ_{st}, implied by Figs. 4 and 5, simply are not borne out by the computations, either not at all [23], or if so, only at quite small values of χ_{st}. This is surprising because of the good agreement with experiment in predictions of extinction [11] and of NO_x scaling [5] by the asymptotics. Further study of the source of the discrepancy with the counterflow computations is needed.

Integration of $\hat{\omega}$ over the parabola can provide an estimate of the total rate of production of NO per unit depth per parabolic flamelet as $\bar{\omega} = 4 \int_0^{S_q} \hat{\omega} l (1 + (\kappa x)^2)^{-1/2} dS$ (mol/cm s), where the factor of four occurs because of the two sides of the parabola and the two moles of NO resulting from each initiation step. Resulting values for l = 2 cm are about 10^{-5}, 2×10^{-6}, 10^{-6} and 5×10^{-7} for κl = 2, 10, 20 and 40, ($Pe \approx$ 6, 30, 60 and 120), respectively and about 6×10^{-7}, 2×10^{-6}, and 10^{-5} for l = 1, 2 and 5 cm, respectively, at κ = 5 cm^{-1} ($Pe \approx 30$). These numbers indicate that larger curvature κ and smaller thicknesses l lead to smaller total production rates, as expected because of the consequent smaller arc length S_q to extinction. The contributions from the prompt, nitrous-oxide and Zel'dovich mechanisms to this total are found to be more than 85%, less than 10% and less than 5%, respectively. The prompt percentage could be much less (and the total correspondingly reduced) if the asymptotics were to strongly overestimate prompt, as suggested above, but the nitrous-oxide contribution would still exceed that of Zel'dovich, which may be surprising, in view of a recent review [25], although our curved flames are relatively highly strained and therefore cooler (see Fig. 3), favoring a smaller thermal contribution.

It has been suggested [26] that turbulence can be described as a collection of Burgers' vortices having lengths about six times their diameters. If this is true, and if each of the vortices has a parabolic flamelet of the type analyzed here wrapped partially around it, then the total NO_x production rate per vortex can be obtained from the proceeding results by simply multiplying by the average vortex length. The number density of vortices would then have to be known to calculate local average production rates. Thus, more research is needed if the present results are to be applied to turbulent combustion.

Conclusions

Estimates of rates of production of oxides of nitrogen in curved flamelets can be obtained by asymptotic methods if a parabolic-flamelet approximation is introduced. At low strain rates the thermal mechanism is dominate at the flame tip, but its rate diminishes with increasing distance from the tip, while the prompt and nitrous-oxide rates increase. Under most conditions, the prompt mechanism dominates the flamelet, and the nitrous-oxide rate exceeds the thermal rate. Two-step reduced main-flame chemistry seems adequate for NO_x estimates, but assumptions of the prompt chemistry at higher strain rates need further study.

Acknowledgments

We especially wish to thank W. T. Ashurst for his many helpful discussions. This research was funded by the United States Department of Energy through the Office of Basic Energy Sciences, Division of Chemical Sciences, and by the Swedish National Board for Industrial and Technical Development.

References

[1] Miller, J. A., and Bowman, C. T., *Prog. Energy Combust. Sci.* 15:287–338 (1989).

[2] Michaud, M. G., Westmoreland, P. R. and Feitelberg, A. S., *Twenty-Fourth Symposium (International) on Combustion*, The Combustion Institute, Pittsburgh, 1992, pp. 879–887.

[3] Glarborg, P., Lilleheie, N. I., Byggstøyl, S., Magnussen, B. F. Kilpinen, P., and Hupa, M., *Twenty-Fourth Symposium (International) on Combustion*, The Combustion Institute, Pittsburgh, 1992, pp. 889–898.

[4] Liñán, A., and Williams, F. A., *Fundamental Aspects of Combustion*, Oxford University Press, New York, 1993.

[5] Røkke, N. A., Hustad, J. E., Sønju, O. K., and Williams, F. A., *Twenty-Fourth Symposium (International) on Combustion*, The Combustion Institute, Pittsburgh, 1992, pp. 385–393.

[6] Ashurst, Wm. T., in *Numerical Combustion* (Derivieux, A., and Larrouturou, B., Eds.), Lecture Notes in Physics Vol. 351, Springer-Verlag, New York, 1989, p. 3.

[7] Ashurst, Wm. T., and Williams, F. A., *Twenty-Third Symposium (International) on Combustion*, The Combustion Institute, Pittsburgh, 1990, pp. 543–550.

[8] Marble, F. E., in *Recent Advances in the Aerospace Sciences* (C. Casci, Ed.), Plenum, 1985, p. 395.

[9] Karagozian, A. R., and Marble, F. E., *Combust. Sci. Techno.* 45:65–84 (1986).

[10] Card, J. M., Ashurst, Wm. T., and Williams, F. A., to appear in *Combust. Flame* (1994).

[11] Seshadri, K., and Peters, N., *Combust. Flame* 73:23–44 (1988).

[12] Williams, F. A., *Combustion Theory*, Addison-Wesley, Menlo Park, CA, 2nd edition, 1985.

[13] Rogg, B., and Peters, N., (Eds.), *Reduced Kinetic Mechanisms for Applications in Combustion Systems*. Lecture Notes in Physics Vol. m15, Springer-Verlag, New York, 1993.

[14] Smooke, M. D., (Ed.), *Reduced Kinetic Mechanisms and Asymptotic Approximation for Methane-Air Flames*, Lecture Notes in Physics Vol. 384, Springer-Verlag, New York, 1991.

[15] Hanson, R. K., and Salimian, S., in *Combustion Chemistry* (W. C. Gardiner, Jr., Ed.), Springer-Verlag, New York, 1984, p. 361.

[16] Michael, J. V., and Lim, K. P., *J. Chem. Phys.* 97:3228–3234 (1992).

[17] Peters, N., and Williams, F. A., *Combust. Flame* 68:185–207 (1987).

[18] Chelliah, H. K., and Williams, F. A., *Combust. Flame* 80:17–48 (1990).

[19] Card, J. M., and Williams, F. A., *Combust. Sci. Techno.* 84:91–119 (1992).

[20] Card, J. M., and Williams, F. A., *Combust. Flame* 91:187–199 (1992).

[21] Lewis, G. S., Cantwell, B. J., Vandsburger, U., and Bowman, C. T., *Twenty-Second Symposium (International) on Combustion*, The Combustion Institute, Pittsburgh, 1988, pp. 515–522.

[22] Drake, M. C., and Blint, R. J., *Combust. Flame* 83:185–203 (1991).

[23] Nishioka, M., Nakagawa, Y., Ishikawa, Y., and Takeno, T., NO Emission Characteristics of Methane Air Double Flame, unpublished, 1993.

[24] Chelliah, H. K., Law, C. K., Ueda, T., Smooke, M. D., and Williams, F. A., *Twenty-Third Symposium (International) on Combustion*, The Combustion Institute, Pittsburgh, 1990, pp. 503–511.

[25] Bowman, C. T., *Twenty-Fourth Symposium (International) on Combustion*, The Combustion Institute, Pittsburgh, 1992, pp. 859–878.

[26] Ashurst, Wm. T., Checkel, M. D., and Ting, D. S.-K., submitted to *Combust. Sci. Techno.* (1993).

List of Tables

List of Figures

Table 1: Rate Constants Associated with the Simplified Mechanism

Step	Reaction	A_j	n_j	E_j
$1f$	$H + O_2 \rightarrow OH + O$	2.000×10^{14}	0.00	70.30
$1b$	$OH + O \rightarrow O_2 + H$	1.568×10^{13}	0.00	3.52
$2f$	$O + H_2 \rightarrow OH + H$	5.000×10^{4}	2.67	26.30
$2b$	$OH + H \rightarrow H_2 + O$	2.222×10^{4}	2.67	18.29
$3f$	$OH + H_2 \rightarrow H_2O + H$	1.000×10^{8}	1.60	13.80
$3b$	$H_2O + H \rightarrow OH + H_2$	4.312×10^{8}	1.60	76.46
$5f$	$H + O_2 + M^a \rightarrow HO_2 + M^a$	2.300×10^{18}	−0.80	0
$18f$	$CO + OH \rightarrow CO_2 + H$	4.400×10^{6}	1.50	−3.10
$18b$	$CO_2 + H \rightarrow CO + OH$	4.956×10^{8}	1.50	89.76
$38f$	$CH_4 + H \rightarrow CH_3 + H_2$	2.200×10^{4}	3.00	36.60
Z	$O + N_2 \rightarrow NO + N$	1.50×10^{13}	0.30	315.0
N[c]	$O + N_2 + M^b \rightarrow N_2O + M^b$	1.16×10^{13}	0.00	81.85
P	$CH + N_2 \rightarrow HCN + N$	3.00×10^{11}	0.00	56.92

Specific reaction-rate constants are $k_j = A_j T^{n_j} \exp(-E_j/R^oT)$; units are moles, cm, s, K, and kJ/mole.

[a] Chaperon efficiencies are taken from [13].

[b] Average chaperon efficiencies are taken to be 1.

[c] Rate constant derived from Ref. [2] using thermodynamic data.

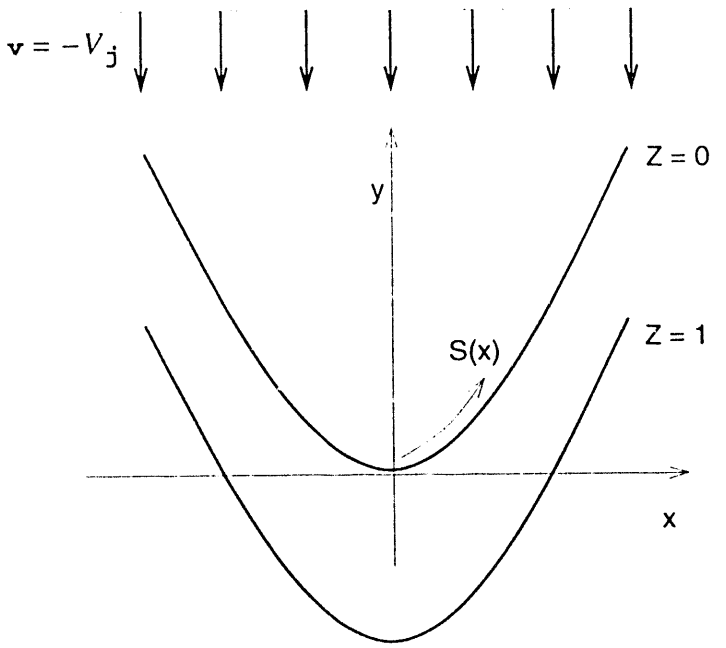
v = −V_j
Z = 0
y
Z = 1
S(x)
x

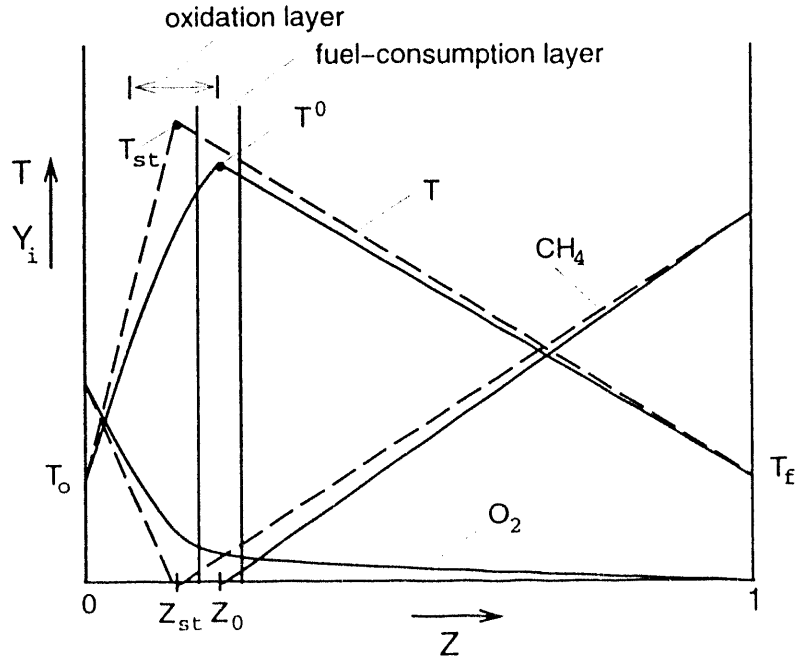
oxidation layer
fuel–consumption layer
T⁰
T_st
T
T
Y_i
CH4
T_o
T_f
O2
0
Z_st
Z_0
1
Z

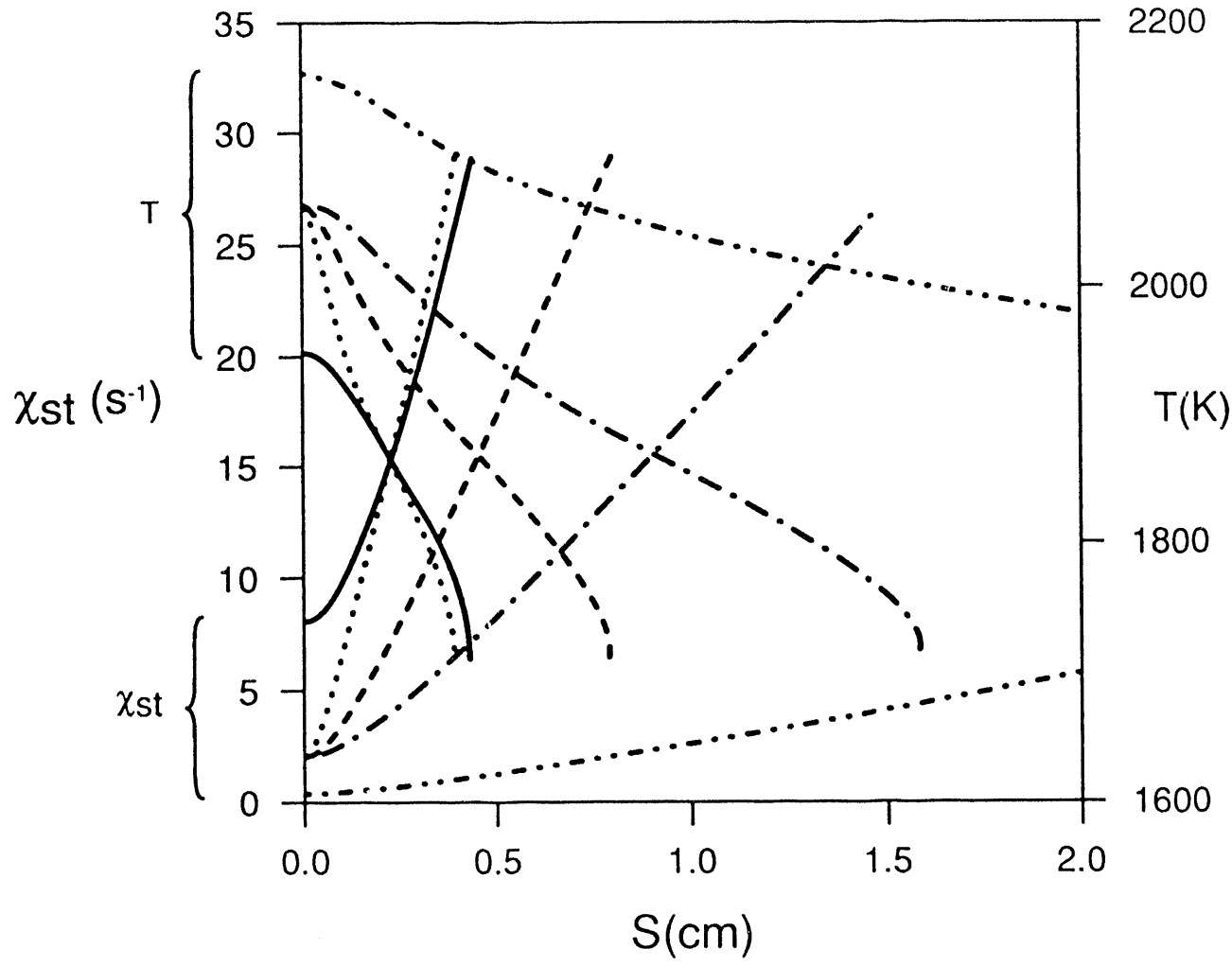
35
30
25
20
15
10
5
0
T
χst
χst (s-1)
2200
2000
1800
1600
T(K)
0.0
0.5
1.0
1.5
2.0
S(cm)

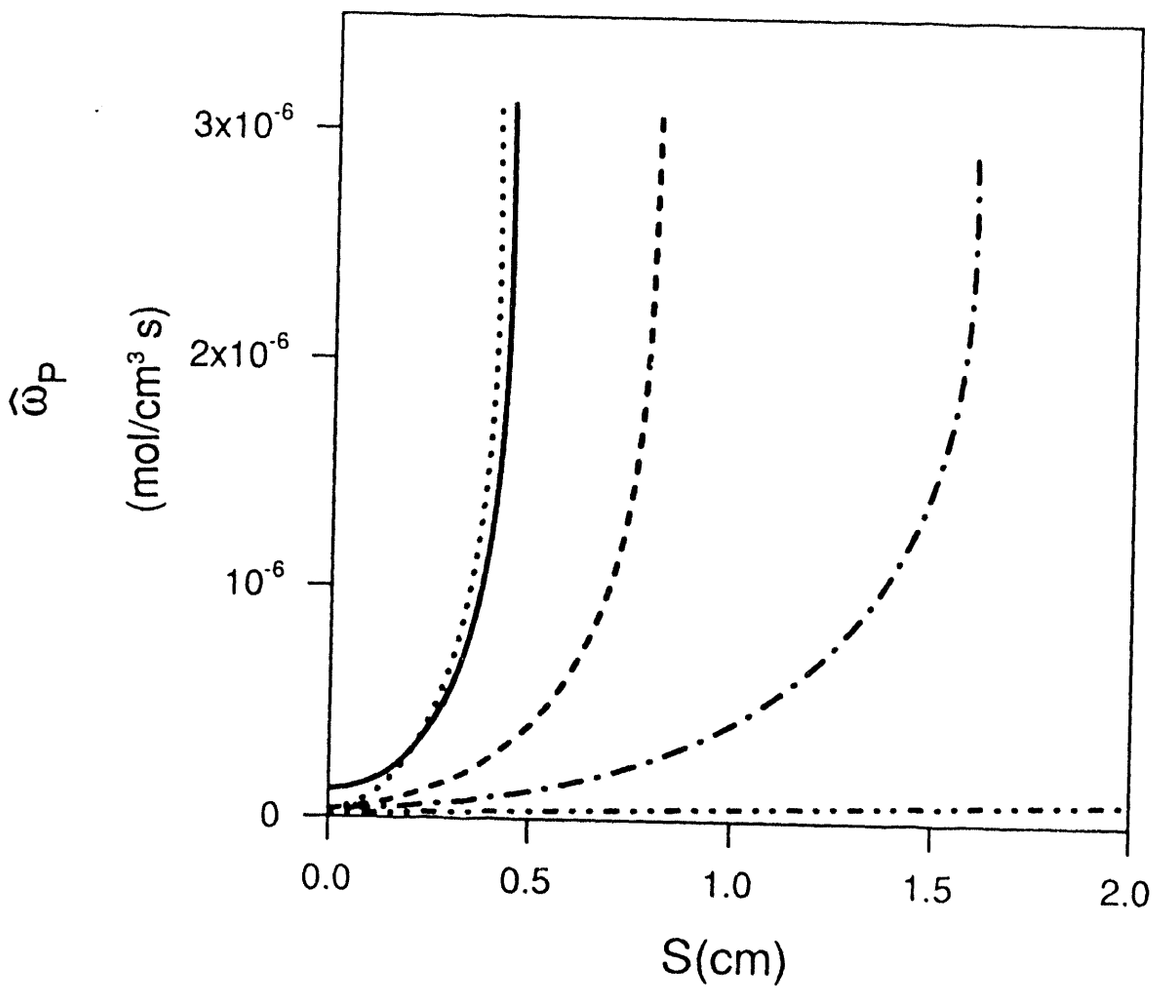
$\hat{\omega}_P$
(mol/cm^3 s)
3x10^{-6}
2x10^{-6}
10^{-6}
0
0.0
0.5
1.0
1.5
2.0
S(cm)

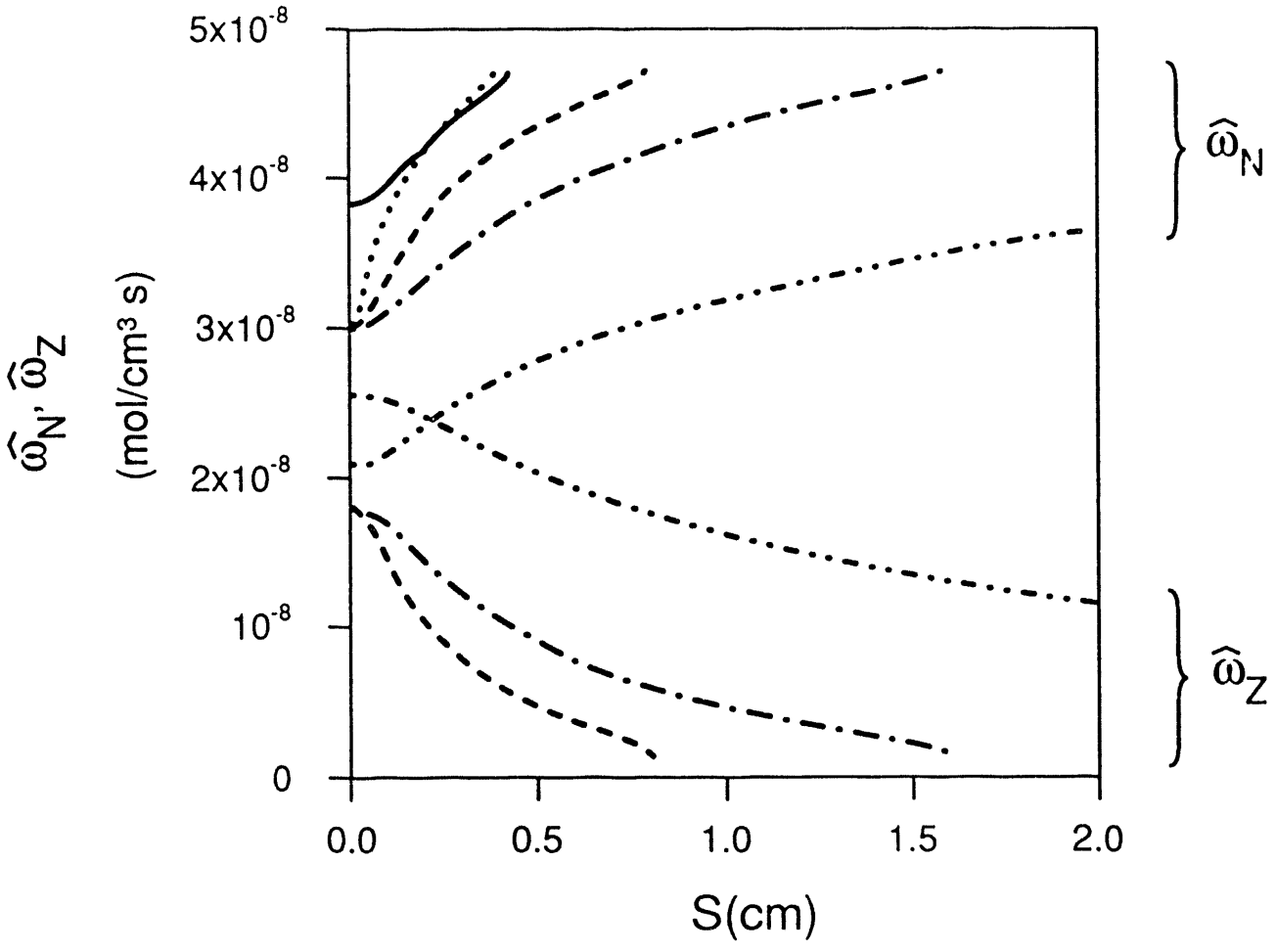
5x10-8
4x10-8
3x10-8
2x10-8
10-8
0
0.0
0.5
1.0
1.5
2.0
S(cm)
ω̂N, ω̂Z
(mol/cm3 s)
ω̂N
ω̂Z

DATE

FILMED

7/7/94

END